

sensitivity, which is defined by the dielectric film structure of the sensor pad. The calculation is based on an effective index model for the dielectric waveguide sensor pad. Thus the experimental value is in good agreement with the theoretically expected phase shift $\Delta\phi_{cal} = 5.05\pi$, calculated for the TE₀ mode.

The resolution of the refractometer chip was determined by measuring the detector signal drift with the measurement cell placed on top of the Mach-Zehnder interferometer bar and with a continuous flow of analyte A. Using a linear fit, the phase drift was determined to be 39mrad min⁻¹, which corresponds to a refractive index resolution of 1.3×10^{-5} for a measurement period of 1 min.

Current work is focusing on the realisation of a monolithically integrated immunosensor chip [6] with applications in medical diagnostics, food analysis or environmental control. The phase-modulator can be used for phase-shifting interferometry, intensity drift compensation of the DBR laser and determination of the sign of refractive index change [3]. Also, multi-sensor arrays and on-chip referencing can be realised with this monolithically integrated optical refractometer chip.

Acknowledgments: The authors are grateful to B. Graf, D. Jeggle, R. Widmer and H. Schütz for processing assistance, H.P. Schweizer for crystal growth, M.T. Gale and K. Dransfeld (Universität Konstanz) for their generous support.

© IEE 1997

Electronics Letters Online No: 19970617

21 March 1997

B. Maisenhölder, H.P. Zappe, M. Moser, P. Riel and R.E. Kunz (Paul Scherrer Institute, Badenerstrasse 569, 8048 Zurich, Switzerland)

J. Edlinger (Balzers AG, 9596 Balzers, Liechtenstein)

References

- 1 STAMM, C., and LUKOSZ, W.: 'Integrated optical difference interferometer as refractometer and chemical sensor', *Sens. Actuators B*, 1993, **11**, pp. 177-181
- 2 LECHUGA, L.M., LENFERINK, A.T.M., KOOYMAN, R.P.H., and GREVE, J.: 'Feasibility of evanescent wave interferometer immunosensors for pesticide detection: chemical aspects', *Sens. Actuators B*, 1995, **24-25**, pp. 762-765
- 3 KUNZ, R.E.: 'Totally integrated optical measuring sensors', *Proc. SPIE*, 1992, **1587**, pp. 98-113
- 4 MAISENHÖLDER, B., ZAPPE, H.P., KUNZ, R.E., RIEL, P., MOSER, M., and EDLINGER, J.: 'A GaAs/AlGaAs refractometer platform for integrated optical sensing applications', to be published in *Sens. Actuators B*, 1997, **38/1-3**
- 5 HOFSTETTER, D., ZAPPE, H.P., and EPLER, J.E.: 'Ridge waveguide DBR laser with nonabsorbing grating and transparent integrated waveguide', *Electron. Lett.*, 1995, **31**, pp. 980-982
- 6 MAISENHÖLDER, B., ZAPPE, H.P., KUNZ, R.E., RIEL, P., MOSER, M., and DUVENECK, G.L.: 'A GaAs/AlGaAs - based Mach-Zehnder interferometer as integrated optical immunosensor', *Proc. SPIE*, 1996, **2928**, pp. 144-152

Circular synthetic aperture radar (C-SAR) system for ground-based applications

A. Broquetas, R. De Porrata, Ll. Sagués, X. Fàbregas and Ll. Jofre

Indexing terms: Synthetic aperture radar, Radar

The authors present an SAR system capable of obtaining radar images from measurements carried out with antennas that describe a circular trajectory centred outside the target region. The analytical formulation of the processor is presented along with its ground range and azimuth resolutions. Some experimental results obtained in an anechoic chamber are also shown.

Introduction: Most of the existing SAR systems are airborne or spaceborne. Ground-based SAR systems, however, are better

suited for short-range applications such as surface scattering studies or buried object detection where very high spatial resolutions are required. In contrast to airborne and spaceborne SAR, wherein the whole platform usually describes a linear trajectory, in truck-mounted or tower-mounted SAR, while only the antenna moves the rest of the system remains static. The mechanical implementation of a linear trajectory for the antenna (L-SAR) therefore becomes difficult. The C-SAR system presented here simplifies this problem by allowing the antenna to describe a circular trajectory around a rotating vertical mast.

Circular geometries for SAR have been extensively studied when the target is in the centre of the antenna path, for example in the spotlight and inverse SAR configurations [1]. However in this case the target is outside the antenna trajectory, allowing an angular high resolution scan of the surface around the radar site.

A continuous wave stepped frequency scan has been used in order to achieve a wide bandwidth, thus the inputs of the C-SAR reconstruction algorithm are the coherent measurements of the scattered field against frequency and azimuth angle.

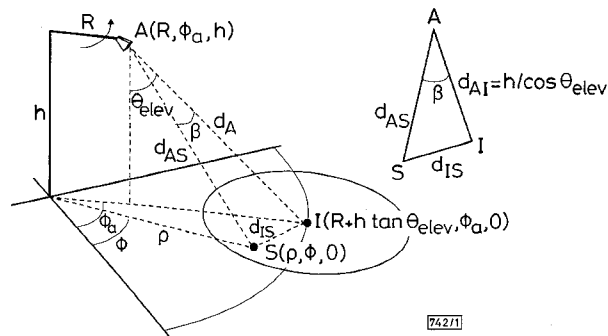


Fig. 1 Geometry of imaging system

C-SAR processor: The geometry of a C-SAR system is illustrated in Fig. 1 in cylindrical co-ordinates. The scatterer, located at point S, remains stationary at a position (ρ, ϕ) of the xy plane. The antennas are located at (R, ϕ_a, h) and point at I, the centre of the illuminated area, with an off-nadir elevation angle of θ_{elev} . Assuming that the target is formed by a distribution of non-directional and independent scatterers of reflectivity $\psi(\rho, \phi)$, the complex value of the field scattered back to the receiver will be given by the coherent addition of the contributions associated with each scatterer:

$$E_s(f, \phi_a) = \int_0^{\infty} \int_0^{2\pi} E_{0s} \psi(\rho, \phi) \frac{e^{-j\frac{4\pi}{\lambda} d_{AS}}}{d_{AS}^2} \rho d\phi d\rho \quad (1)$$

where

$$d_{AS} = \sqrt{R^2 + \rho^2 - 2R\rho \cos(\phi - \phi_a) + h^2} \quad (2)$$

is the distance between the antennas and the scatterer, and E_{0s} is a constant that depends, among others, on parameters of the system such as antenna gain and transmitted power. Since this constant will be normally removed by external calibration using a reference target, it will not henceforth be considered.

The objective of the imaging system will be the reconstruction of the reflectivity map from a set of measurements $E_s(f, \phi_a)$ at different frequencies and angles. In mathematical terms this can be achieved by applying a focusing operator to the measured fields:

$$\hat{\psi}(\rho', \phi') = \int_0^{\infty} \int_0^{2\pi} E_s(f, \phi_a) \xi(f, \phi_a, \rho', \phi') d\phi_a df \quad (3)$$

where $\xi(f, \phi_a, \rho', \phi')$ is the kernel function to be found, hence the image $\hat{\psi}(\rho', \phi') = \psi(\rho, \phi)$. For a given scene point (ρ', ϕ') , $\xi(f, \phi_a, \rho', \phi')$ should 'focus' all the performed measurements on this point by generating the argument and amplitude that the wave has 'lost' on its way to and back from the scatterer located at (ρ, ϕ) . The proposed solution is therefore

$$\xi(f, \phi_a, \rho', \phi') = e^{j\frac{4\pi}{\lambda} \sqrt{R^2 + \rho'^2 - 2R\rho' \cos(\phi' - \phi_a) + h^2}} \times [R^2 + \rho'^2 - 2R\rho' \cos(\phi' - \phi_a) + h^2] f \quad (4)$$

If $R \rightarrow \infty$, eqn. 5 becomes the conventional linear SAR reconstruction implying a quadratic phase with respect to the antenna displacement.

With good signal to noise ratios (≥ 20 dB), the effects of the radiation diagrams of both transmitter and receiver antennas $G_T(\beta)$ and $G_R(\beta)$ can be taken into account and corrected in the reconstruction by multiplying $\xi(f, \phi_a, \rho', \phi)$ by

$$\frac{1}{G_T(\beta)G_R(\beta)}$$

within the beamwidth of the antenna. The angle β is shown in Fig. 1 and can be expressed against geometric parameters of the system. For this purpose, $G_T(\beta)$ and $G_R(\beta)$ can be modelled by using a Gaussian or parabolic approximation.

An advantage of compensating the amplitude terms of the target range and gain of antennas in the focusing kernel ξ is that the sensitivity becomes invariant across the image field. The shape of an imaged point scatterer (point spread function) depends on the target range, although it has been found approximately invariant in short range numerical simulations.

Image resolution: The range resolution ΔR depends on the time pulse resolution $\Delta \tau$, which is the inverse of the bandwidth system $B = f_{max} - f_{min}$ [1]. The resolution in slant range ΔR and ground range ΔR_g are given by [1]:

$$\Delta R = \frac{c\Delta\tau}{2} = \frac{c}{2B} \quad (5)$$

$$\Delta R_g = \frac{c}{2B \sin(\theta_{elev})} \quad (6)$$

The azimuth resolution ΔS of the C-SAR system is defined as the ability to discriminate two close radar targets which are located at the same arc, and it can be calculated from the Doppler frequency resolution Δf_d [1]:

$$\Delta S = \frac{c}{4f_{max}} \frac{\sqrt{R^2 + \rho^2 - 2R\rho \cos(\Delta\theta_H/2) + h^2}}{R \sin(\Delta\theta_H/2)} \quad (7)$$

where $\Delta\theta_H$ is the 3dB beamwidth of the antennas.

If the antennas present a high directivity ($\Delta\theta_H < 20^\circ$) and $R \rightarrow \infty$, the azimuth resolution $\Delta S \approx l/2$, which is the conventional linear SAR azimuth resolution, l being the dimension of the antenna. In contrast to linear SAR, the azimuth resolution degrades with range because the length of the synthetic aperture does not increase proportionally. The optimal elevation angle is that where both resolutions are equal, and it can be calculated by equating eqns. 6 and 7:

$$\theta_{elev_{opt}} = \tan^{-1} \left[\frac{R}{h} \frac{f_{max}}{B} \Delta\theta_H \right] \quad (8)$$

Measurement results: Several multifrequency measurements have been undertaken in the X-band at the electromagnetic anechoic chamber of the Universitat Politècnica de Catalunya (UPC). The measurement system is basically a vector network analyser based scatterometer using two closely spaced antennas placed at the end of a 0.9m metallic bar mounted on an azimuth positioner. The transmit-receive antennas were two rectangular horns located at a height of 1.95m, with an off-nadir elevation angle of 45° . A personal computer controlled the scatterometer to perform a frequency sweep for each angular sample point.

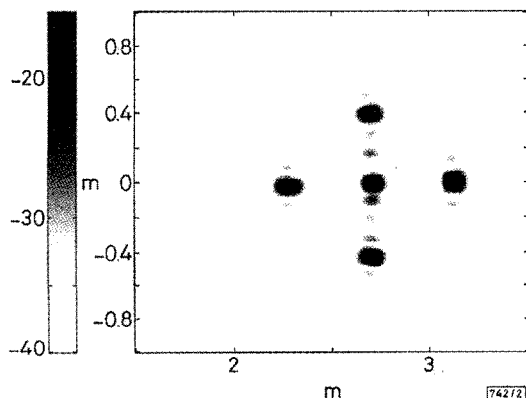


Fig. 2 Reflectivity image of five trihedrals

Fig. 2 shows the reconstructed image for horizontally polarised copolar data sampled over 161 angular points measured from 12 to 16GHz with a frequency interval of 10MHz. This image corresponds to five identical small trihedrals spread on the ground of the anechoic chamber. The quasi-space invariance as well as the uniform sensitivity can be observed in this image.

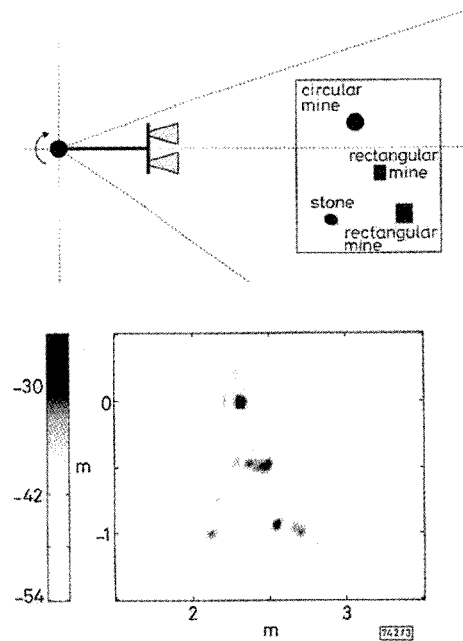


Fig. 3 Experimental setup and obtained reflectivity image

An important potential application of the C-SAR system is buried object detection, such as for anti-personnel plastic mines. In this case, frequencies in the range 0.5–4GHz would be preferred in order to obtain some terrain penetration. However, a preliminary experiment at higher frequencies has been carried out to assess the imaging capabilities of dielectric objects laid on a ground surface. In this context, three plastic mine equivalent objects of different sizes (5, 10, 20cm) and a stone (10cm) were spread over a large region of sandy simulated soil inside the anechoic chamber (Fig. 3). The measurement was carried out with HH polarisation, 161 points in azimuth and sweeping from 12 to 18GHz with a frequency interval of 15MHz. Fig. 3 shows the reconstructed SAR image. As we can see, the three mines are detected above the ground clutter and the stone level and located at its exact position. Note that the biggest mine is larger than the image resolution cell and presents two distinguishable bright points.

Conclusions: A circular synthetic aperture radar processor has been presented and evaluated. This system has been designed in order to obtain radar images using a ground-based scatterometer where only the antennas move describing a circular trajectory. Although the formulation and implementation are more complicated than a conventional linear SAR, the experimental setup is considerably simplified. The results show evidence of the applicability of this approach to very high resolution surface scattering analysis and buried objects detection.

Acknowledgments: This work has been supported by the Spanish Commission for Science and Technology CICYT TIC 96-0879.

© IEE 1997
Electronics Letters Online No: 19970635

24 March 1997

A. Broquetas, R. De Porrata, Ll. Sagués, X. Fàbregas and Ll. Jofre (Departamento Teoria del Senyal i Comunicacions, Universitat Politècnica de Catalunya (UPC), Campus Nord UPC, D3, 08034, Barcelona, Spain)

References

- 1 WEHNER, D.R.: 'High resolution radar' (Artech House, Norwood, USA, 1997)
- 2 BROQUETAS, A., JOFRE, L., and CARDAMA, A.: 'A near field spherical wave inverse synthetic aperture radar technique'. IEEE Antennas and Propagation Soc. Int. Symp., Chicago, 1992, Vol. 2, pp. 114–117